Biuletyn PAN, Vol. 42, No4, 1994, pp. 541 - 559

METALLURGY

Cutting of Steel Plates by Means of a Continuous-Wave CO_2 Laser. Theory and experiment.

by

Sławomir Maksymilian KACZMAREK, Wojciech PRZETAKIEWICZ, Józef RAFA and Andrzej PAWLATA

Presented by B. CISZEWSKI on April 11, 1994

Summary. An analysis has been carried out an analysis of the characteristics of the laser cutting process resulting from the time-dependent solution of the heat conductivity equation inside the steel sheet. It has been assumed that the laser beam has a Gaussian spatial shape. The heat conductivity equation and boundary conditions have been derived for a 3-D sheet moving with a constant velocity *v* in a direction *x*.

1. **Introduction**. In laser cutting, laser welding and laser toughening CO_2 CW lasers are usied. Necessary power densities are achieved at with much greater watt-hour efficiency and about twice less costs comparing to Nd:YAG laser.. Actually lasers with power of 500-1500 W (and even about 2500 W) are applyed. There are used pulse CW lasers to cut materials into complex shapes. Steel sheets of 10 mm thickness are allowed.

1.1 Denotations:

laser beam: λ - beam wavelength, 2Φ - beam divergence, P - beam Power, ρ_0 - power density at a beam focus, f- focal length of a lense, d_0 - diameter of focused beam, $w_o=d_o/2$, $2\cdot g$- depth of focus, r_0 - laser Gaussian beam radius $w_0 = d_0/2$, B - spot size,

material: ρ - density, c - specific heat, D- heat diffusivity, $D=K/\rho\cdot c$, K - heat conductivity, A - absorption, T_m - melting point, R_z - surface roughness,

Key words: temperature distribution from external heat sources, laser cutting of steel sheets

process: p - gas pressure, L - sheet thickness, v - sheet velocity, z_0 - beam focus distance from material surface, w-width of the cutting, HAZ-width of heat affected zone.

model:α, β- real coordinates for Fourier transforms, t - time, x,y,z - space coordinates, s - Laplace coordinate, q_V - voluminal efficiency of internal heat sources, N - number of area partitions of sources along x - axis, M - number of area partitions of sources along *z* axis.

2. Experimental details. The focused laser beam of a diameter $2r_0$ perpendicular to the surface of steel sheet of thickness L, moving with a velocity v in the x - direction, causes the sheet cutting of a width *w* (Fig.1). The length and width of the sheet are much greater than its thickness [1]. An O_2 flux was used to assist.

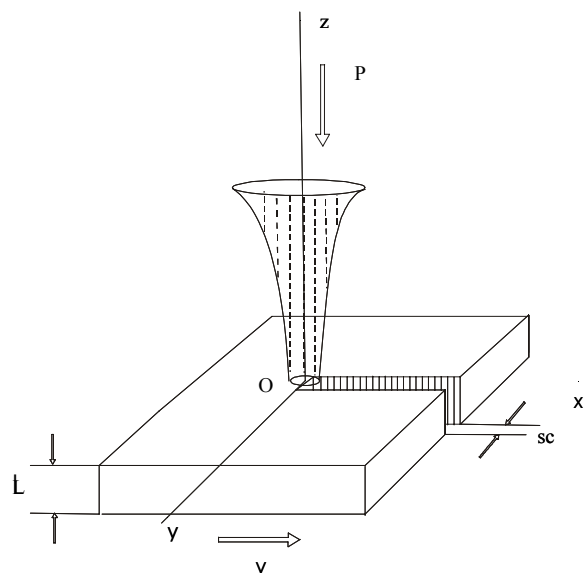

Fig. 1. Configuration of a metal sheet cut by a laser beam in a system of coordinates

In our investigations we have used two types of steel sheets:

1. St3SCuX steel sheet with 3mm thickness [0.18%C],
2. MSt1 steel sheet with 2.5mm thickness [0.04%C].

The first steel sheet was cutted at constant power 700 W and at a constant velocity v = 1400 mm/min. The aim was to find optimal beam focus position for the best cutting and the narrow cutting slot. It was stated that the beam focus is localised at z_0 = - 0.2 mm (z = 0 on the upper surface of the sheet) [2].

The second steel sheet was cut at the constant focus of z_0 = - 0.2 mm and differing powers: P = 500W, 700W, 900W and velocities: v=720 mm/min, 1000 mm/min, 1400 mm/min, 2000 mm/min. Dependence of P and v on the width of the cut was measured for a given sheet thickness.

Parameters of

- laser beam: beam wavelength λ=10.6μm, beam power: P = 500, 700, 900W, beam divergence $2\cdot\Phi$ = 4 mrad, multimode laser beam, polarization - eliptical.

- focusing lens : focal length (ZnSe) f=96mm, spot size B=25mm.

- focusing laser beam : density power at a focus ρ_0 = from $4.4\cdot10^5$ W/cm^3 for P=500W to $7.9\cdot10^5$ W/cm^3 for P=900W, diameter of focused beam $d_0 = 2r_0$ about 0.4mm, depth of focus $2\cdot g$ = 21.4 mm.

- assisting gas: O_2 , gas pressure - p = 7 bar.

- material ($T > T_m$), [3 - 5] : absorption A=0.8, heat conductivity K=32 W/m·deg, heat diffusivity D=6 mm^2 /s, melting point T_m =1520°C.

- process : sheet thickness L=3mm for St3SCuX and 2.5mm for MSt1, velocities of sheet feed v=720, 1000, 1400, 2000 mm/min, distance of beam focus from material surface z_0 = - 0.2 mm.

2.1 *Analysis of St3SCuX sheet cutting results*. The cutting was proceeded at the constant laser power P=700 W and the constant cutting velocity v=1400 mm/min. Beam focus position (z_0) was changed step by step in the range -5.2 - +3.8 mm with z=0 corresponding to the top sheet surface. It was found that changes in the cutting width *w* as well as the width of a heat affected zone (HAZ) versus z_0 are smooth functions. It was found that the narrower *w* and the greater HAZ are at the edge of cutting material in case of the beam focus position somewhat below the top sheet surface (for z_0= - 0.2 mm). Tese results confirm those in [6, 7].

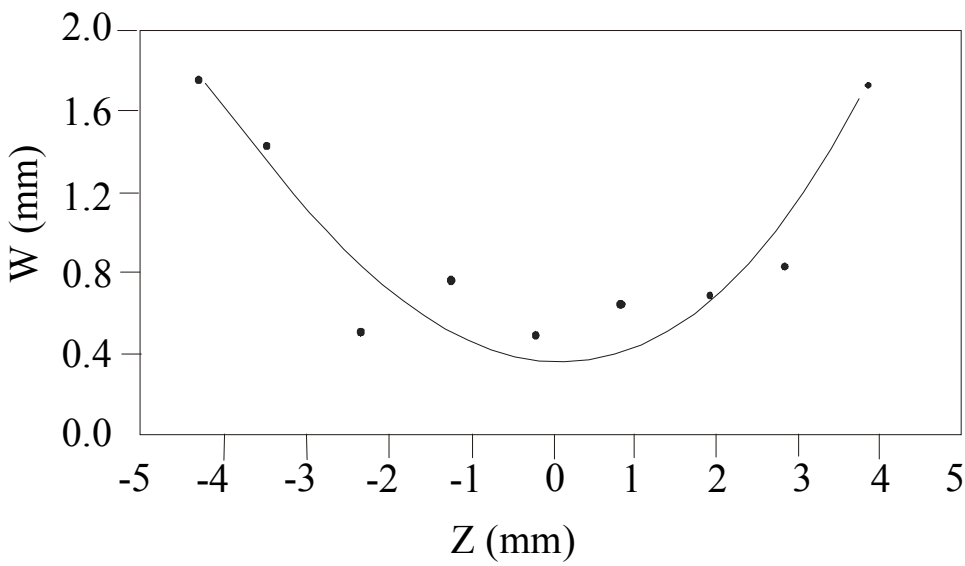

Fig. 2. Dependence of cutting slits on beam focus positions for St3ScuX steel sheet. *P* = 700 W, *v* = 1400 mm/min

Changes of *w* under consideration are shown in Fig. 2, while Fig. 3 presents those for a HAZ changing in a similar way. Under above

conditions the smallest cutting width is about 0.5 mm and the biggest one is 1.8 mm. The position of majority of experimental points in Fig. 2 does not exceed the value of w=+0.7 mm for the whole range from -2 to +2 mm of z_0 .

The size of HAZ was estimated on the base of characteristic structure changes in the layer of the nearby cutting surface. It was found that the boundary of a HAZ is sharply seen and is paralel to the edge of cutting (Fig. 4). The smallest width of a HAZ for the above conditions is equal to 0.1 mm (at z_0= - 0.2 mm) and the biggest one is 0.5 mm (at z_0= - 5.2 mm).

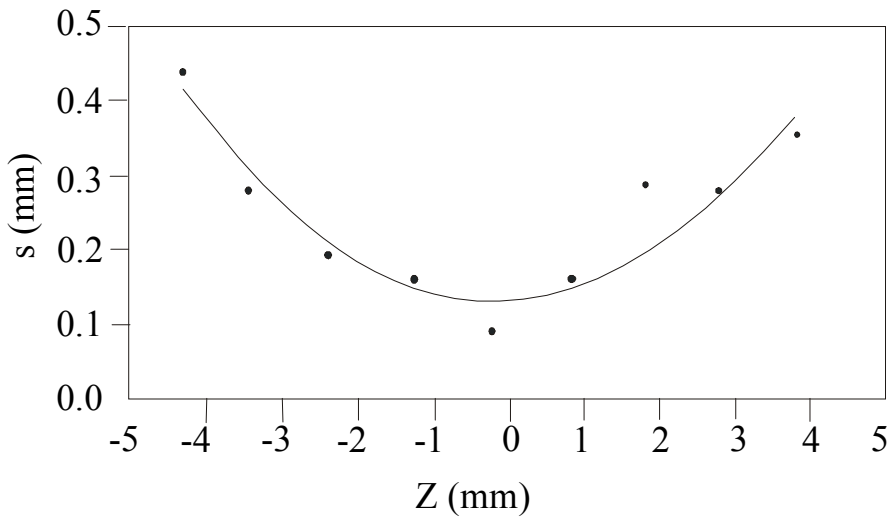

Fig. 3. Effect of beam focus positions on HAZ widths for St3ScuX steel sheet.
P = 700 W, v = 1400 mm/min

Among various materials of interest pearlite (marked at figure as P), being component of initial ferritic-pearlitic structure, transforms into martensite (marked by M). So, the hardening takes place near the surface zone. The characteristic "sharp" intercristallic coarse of the HAZ boundary line was found (Fig. 4b).

Different widths of HAZ for different values of the z_0 prove the existence of different maximal values of temperatures in the cutted material range.The greater temperature during the cooling, the more coarse grain structure of martensite at the near-edge zone and it favours the forming the most visible but generally thin oxide layer about 4 μm thickness.

In case of the cutting with a beam focus below the top sheet surface, the narrow cutting width and HAZ, as well as the best quality (smoothness) of surface under the cutting have been obtained. In Fig. 5a and in Fig. 5b, there have been shown respectively the examples of different quality of this surface for z_0 equal to -0.2 mm and +2.8 mm, and for the roughness R_Z in ranges 70-100 μm and 400-500 μm.

Characteristic striae seen in this figure are due to the folding of melted material [6, 7].

The profile and roughness of surface under the cutting were dependent on the gas pressure and velocity of cutting. It is easy seen that the frequency of the occurring of the characteristic striae increases and the heights of corresponding perturbances decreases due to the approach the top sheet surface by the beam focus, when the remaining parameters are constant. Material infiltrations at the bottom sheet edge leads to greater roughness (Fig. 5b).

2.2 *Analysis of MSt1 sheet cutting results*. The laser powers P are 500, 700 and 900 W and the cutting velocitiesare: 520, 720, 1000, 1400 and 2000 mm/min (z_0=-0.2 mm). The smoothness of the cutting surface is greater than in the previous case, and easy seen when compare Fig. 5 and 6 where are the cutting surfaces mostly differentiating each other by microgeometry.

In Fig. 6a there is seen the surface of MSt1 sheet while in Fig. 5a the St3SCuX sheet cutted in the same conditions (P=700 W, v=1400 mm/min, z_0 = - 0.2). Quality of both the surfaces is similar.

In Fig. 6b there is the cutting surface of MSt1 sheet obtained at the same P and z_0 except of the velocity v=2000 mm/min. The increase of the cutting velocity does not affect a frequency of striae according to the prediction in [6], but it causes the bending of slits in the direction opposite to the direction of their creation, and the increase of surface roughness R_z in range 100-150 μm especially near the bottom cutting edge.

2.3 *Effect of change of laser power*. It was found that, from the three different laser powers, the smallest value of *w* can be obtained at the intermediate one 700W, especially for v exceeding 1000 mm/min (Fig. 7).

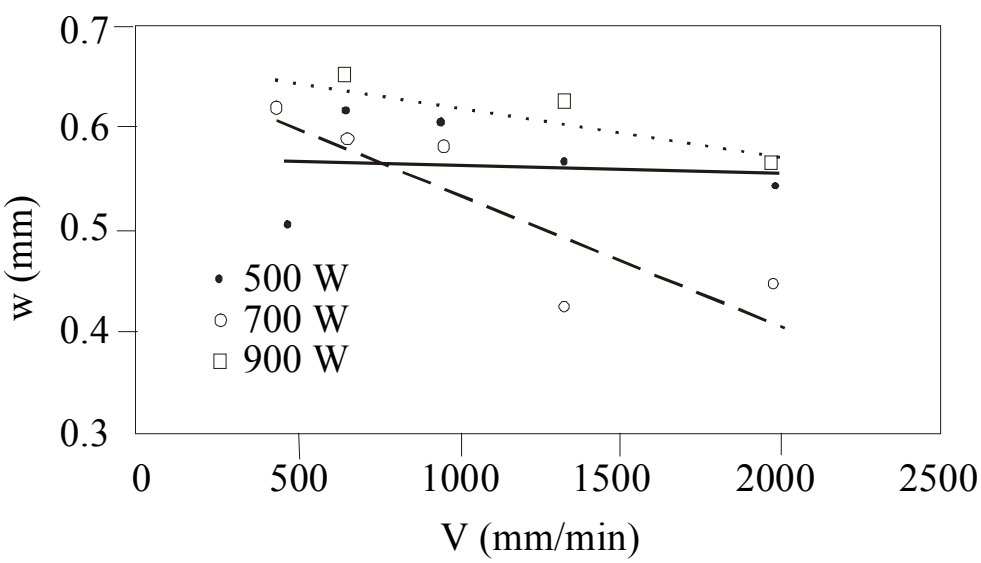

Fig. 7. Dependence of salt widths w on the cutting velocity v for various laser powers for MSt1

The increase of P within the respective range results in increase of the average width of the HAZ at the near-edge layer (Fig. 8a). However, for the specified laser power, changes of this zone width versus v are not monotone (Fig. 8b).

For the particular laser power differencies among the HAZ values are the smallest at v equal to 2000 mm/min, but greater at v's 1000 and 1400 mm/min.

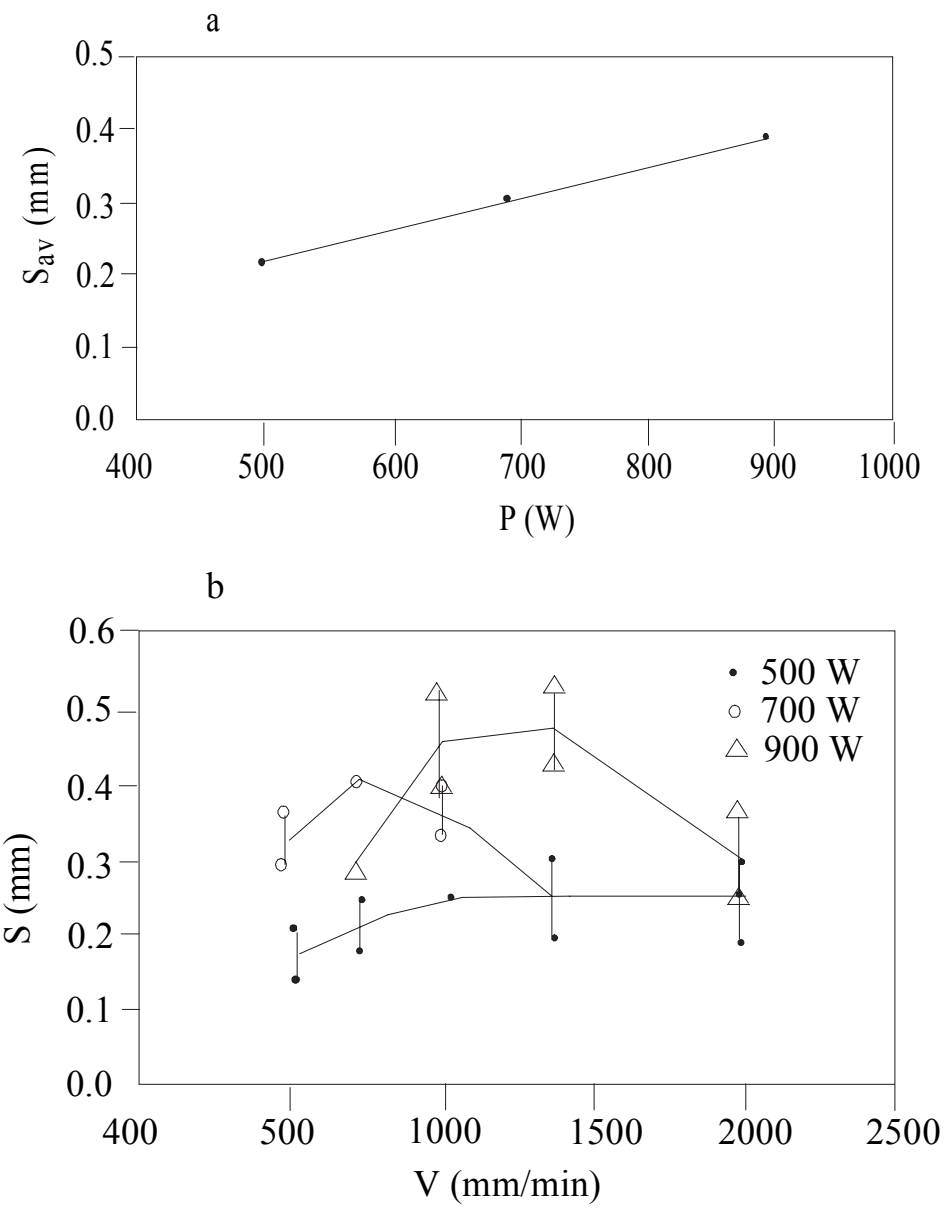

Fig. 8. A – effect of the laser power and b – the cutting velocity on the HAZ width for MSt1

The *HAZ* is characterized by effect of growth of ferrite grain (Fig. 9a). At higher *P* in this zone there are also observed micro-ranges of melted material (Fig. 9b), localized in places of occurring of pearlite or tertiary cementite, as structural components with the appreciable carbon concentration (0.8 and 0.67 %, respectively).

2.4 *Effect of changes of the velovity of laser cutting*. In Fig. 7 one can see that the cutting width decreases when the cutting velocity increases, especially in case of the 700 W laser beam .

In range of the HAZ created as an effect of cutting, rank of ferrite grain growth increase for smaller values of cutting velocities.

The boundary of HAZ in MSt1 steel, with very small carbon contents is not so clear as in St3SCuX steel. That irregular boundary is running across the grain edges and sometimes deflects far inside of material including grain groups, which have undergone expansion. It is because of a non-uniform carbon distribution (cementyte) at a ferritic structure. This involves in turn the locally different possibilities of grain boundary migration.

That result has confirmed the earlier results of laser cutting of an Al - 2% Mg alloy [8]. The irregular resolidification front line, rising at the near-edge zone was realised there as a result of the temperature influence on the strongly packed, material because of rolling. The structure of that material as well as of MSt1 steel is a monophase solid solution with a slight amount of dispersive secretions of intermetallic phases.

The analysis of macrogeometry and microstructure of steel sheets inside the zone of their cutting have arrived at an interesting conclusion. As it has been shown [6, 7], the mechanism of creating of cutting slits during cutting process prevent them from broadening due to the beam self-focusing in a rising capillary. The broadening of the laser beam below its focus gives the 25 to 50% increase of the HAZ width at the bottom sheet surface compared to that at the top surface .

2.5 *Conclusions*. With the laser power 700W and the cutting velocity 1400mm/min and the beam focus position z_0 = -0.2 mm, there was obtained the smallest (about 0.45 mm) slit width *w*, the best quality (smoothness) of the cutted surface (R_Z < 100mm) and the smallest (about 1mm) value of the HAZ .

In the St3SCuX steel with an initial ferritic-pearlitic structure, the HAZ is clearly separated because of the occuring of the phase transformations pearlit ⇒ austenit ⇒ martensite. The boundary of this zone has a transcrystallic character. In the MSt1 steel, on the contrary, the zone of expanded ferrite grains has an irregular shape.

The observed geometry of the cut is determine by the cutting velocity

rather than the laser power. The dependence $w = f(v)$ is opposite, but observed changes are not so important. Values w are bounded at: 0.5-0.6 mm.

The HAZ in the MSt1 steel depends clearly on the conditions of laser treatment. The width of a near-edge zone, where the grain growth occurs, changes from 0.2 to 0.4 mm. The greater laser powers, the greater values of HAZ widths. When the cutting velocity changes from 500 to 2000 mm/min, the HAZ width is mononotone. This dependence has an increase-decrease character.

The both sets of laser parameters are best for the cutting of MSt1 of 2.5mm thickness: P = 700W, v = 1400mm/min, z_0 = - 0.2mm or P = 900W, v = 2000 mm/min, z_0 = - 0.2 mm.

3. Theoretical models. In the literature there were described two models of the laser cutting process in case of the thin steel sheets [9 - 11] were described: a linear source model and an uniform distribution model. With those models we want to describe the laser cutting of thicker steel sheets, up to 10 mm.

First, the time dependent heat conductivity equation for a laser beam of a Gaussian 3-D profile was solved. Then, the five models had been investigated and illustrated for the laser cutting of steel sheets: three "flat models" - with a linear source, an uniform distribution and a 2-D Gaussian distribution, and two "space models" - with a point source and a 3-D Gaussian distribution. Models have a common description of the heating process of the cut sheet, namely, from the volume heat sources located in its interior. In case of the pulsed laser, heat sources are outside the sheet and the description is more complex. In all the models, there are the following assumptions (see Fig.1):

- a source in the origin of a coordinate system x, y at $z = z_0$ ($z = 0$ on the upper surface of the cut sheet),
- a uniformly moving sheet is of the infinite length and width,
- the sheet material is homofeneous, thermal constants of the material do not depend on a temperature ,
- in the "flat models": dT/dz=0,
- the heat flow is quasi-stationary in the z-axis direction,
- the absence of an assisting gas flux.

The equation of heat conduction for the sheet with internal heat sources with power q_V, moving in the x-direction , is as follows [9, 12]

$$\rho \cdot c \cdot \left(\frac{\partial T(x,y,z,t)}{\partial t} + v \cdot \frac{\partial T(x,y,z,t)}{\partial x}\right) = K \cdot \Delta T(x,y,z,t) + q_v, \quad (1)$$

- the boundary condition on the layer surface

$$\frac{\partial T(x,y,z,t)}{\partial z}\Big|_{z=0,L} = 0,$$

- the initial condition :

(2) $$T|_{t=0} = T_0,$$

and the conditions of radiation at infinity

$$(T - T_0) + \mathbf{k} \cdot \mathbf{grad}(T - T_0)\,|_{\substack{|x|\to\infty \\ |y|\to\infty}} \Rightarrow 0,$$

$$\mathbf{k} = (x, y),\ \mathbf{grad}(T) = (\frac{\partial T}{\partial x}, \frac{\partial T}{\partial y}).$$

For the point source model:

(3) $$q_v = \frac{A \cdot P}{L} \cdot \delta(x) \cdot \delta(y) \cdot \delta(z - z_0),$$

for the linear source:

(4) $$q_v = \frac{A \cdot P}{L} \delta(x) \cdot \delta(y).$$

For the uniform beam, 2D and 3D Gaussian distributions, we have [13]:

(5) $$q_v = \frac{A \cdot P}{\pi \cdot r_0^2 \cdot L},$$

(6) $$q_v = \frac{2 \cdot A \cdot P}{\pi \cdot w_0^2 \cdot L} \cdot \exp(-\frac{2}{w_0^2} \cdot (x^2 + y^2)),$$

(7) $$q_v = \frac{2 \cdot P \cdot A \cdot w_0^2}{\pi \cdot w^4(z) \cdot L} \cdot \exp(-\frac{2}{w^2(z)} \cdot (x^2 + y^2)),$$

(8) $$w(z) = w_0 \cdot \sqrt{1 + ((z - z_0) \cdot \lambda / (\pi \cdot w_0^2))^2}.$$

3.1. Time-dependent solution. Taking q_v in the form: $q_v = f(t) \cdot d(x) d(y) \cdot d(z)$, meaning the time-dependent model of the point source, we get after Fourier and Laplace transformation [14]

(9) $$d_z^2 \tilde{\tilde{\theta}} - \kappa^2 \cdot \tilde{\tilde{\theta}} = -\frac{\tilde{f}(s)}{K} \cdot \delta(z - z_0),$$

(10) $$d_z \tilde{\theta}\,|_{z=0,L} = 0,$$

where $i = \sqrt{(-1)}$, d_z-derivative with respect to z,

(11)

$$\kappa^2 = \alpha^2 + \beta^2 + \frac{\rho c}{K}(s + i \cdot \alpha \cdot v),$$

$$\tilde{f}(s) = \int_0^\infty f(t) \cdot e^{-s \cdot t} dt,$$

$$\tilde{T}(\alpha, \beta, z, t) = F_{xy} T(x, y, z, t) = \int_{-\infty}^{\infty}\int_{-\infty}^{\infty} T(x, y, z, t) \cdot e^{-i \cdot (\alpha \cdot x + \beta \cdot y)} dx \cdot dy,$$

$$\tilde{\tilde{T}}(\alpha, \beta, z, s) = A_t \tilde{T}(\alpha, \beta, z, t) = \int_0^\infty T(\alpha, \beta, z, t) \cdot e^{-s \cdot t} dt,$$

$$\theta = T - T_0$$

The solution of the problem described by (9 - 11) can be presented in the following form :

(12) $$\tilde{\tilde{\theta}}(\alpha,\beta,z,s) = \frac{\tilde{f}(s)}{2 \cdot K} \cdot [\sum_{j=1}^{2} \tilde{\tilde{\theta}}_j(\alpha,\beta,z,s) + \sum_{n=0}^{\infty} \sum_{j=3}^{6} \tilde{\tilde{\theta}}_j(\alpha,\beta,z,s)],$$

(13) $z_1 = z + z_0$, $z_2 = |z - z_0|$, $z_3 = z + z_0 + 2 \cdot L \cdot (1+n)$,
$z_4 = z - z_0 + 2 \cdot L \cdot (1+n)$, $z_5 = - z + z_0 + 2 \cdot L \cdot (1+n)$,
$z_6 = - z - z_0 + 2 \cdot L \cdot (1+n)$, $\theta_j(\alpha,\beta,z,s) = \exp(-\kappa z_j)/\kappa$, $j=1..6$,

In order to construct a space-time solution, we apply the Cagniard - de Hoop technique [15] consisting in the parametrization of an integration contour on the complex plain. After some calculations, we obtain a solution for the Laplace transform $\tilde{\theta}_j$ in the form:

(14) $$\tilde{\theta}_j(x,y,z,s) = \frac{e^{x \cdot u^2 \cdot v/2}}{4 \cdot \pi \cdot R_j} \cdot \tilde{f}(s) \cdot e^{-\sqrt{s + u^2 \cdot v^2/4}},$$

(15) $R_j = \sqrt{x^2 + y^2 + z_j^2}$ - a standart distance.

Solution (14) corresponds with the time varying laser - beam power $P(t) = P_0 \cdot f(t)$. In case of the continuous power laser, we get : $P(t) = P_0 \cdot H(t)$, where $H(t)$ is the Heviside function and :

(16) $$\tilde{\theta}_j(x,y,z,s) = \frac{e^{x \cdot u^2 \cdot v/2}}{4 \cdot \pi \cdot R_j \cdot s} \cdot \exp[-\sqrt{s + u^2 \cdot v^2/4}\,(R_j \cdot u)]$$

For the pulsed power laser, we obtain

$P_i(t) = P_0..H(t - t_i) \cdot H(t_{i+1} - t)$, $t_{i+1} > t_i$

$\tilde{\theta}_j = \sum_{i=1}^{I} \tilde{\theta}_{ji}$, where I - amount of laser pulses,

(17) $$\tilde{\theta}_{ji} = \frac{e^{x \cdot u^2 \cdot v/2}}{4 \cdot \pi \cdot R_j \cdot s} \cdot (e^{-s t_i} - e^{-s t_{i+1}}) \cdot e^{-\sqrt{s + u^2 \cdot v^2/4}\,(R_j \cdot u)}$$

By computing the inverse Laplace transforms of solutions (14)-(17), we get

$$(18)\quad \theta_j(x,y,z,t) = \frac{u}{8\cdot(\pi\cdot t)^{3/2}}\cdot \exp\left(-\frac{R_j^2\cdot u^2}{4\cdot t}\right)\cdot \exp[u^2\cdot v/2\cdot(x-v\cdot t/2)],$$

$$\theta_j(x,y,z,t) = \frac{\exp(x\cdot u^2\cdot v/2)}{8\cdot\pi\cdot R_j}\cdot [\exp(-u^2\cdot v\cdot R_j/2)\cdot \mathrm{erfc}\left(\frac{R_j\cdot u}{2\cdot t^{1/2}} - \frac{u\cdot v\cdot t^{1/2}}{2}\right)$$

$$(19)\qquad + \exp(u^2\cdot v\cdot R_j/2)\cdot \mathrm{erfc}\left(\frac{R_j\cdot u}{2\cdot t^{1/2}} + \frac{u\cdot v\cdot t^{1/2}}{2}\right)],$$

$$(20)\qquad \theta_{ji}(x,y,z,t) = \frac{\exp(x\cdot u^2\cdot v/2)}{4\cdot\pi\cdot R_j}\cdot [\theta_j(x,y,z,t-t_i)\cdot H(t-t_i)$$
$$-\theta_j(x,y,z,t-t_{i+1})\cdot H(t-t_{i+1})].$$

For the remining models, we have:
- the solution of equation (1), with q_V equal to (4) and boundary conditions (2), is :

$$(21)\qquad T(x,y) = T_0 + \frac{P\cdot A}{2\cdot\pi\cdot L\cdot K}\cdot \exp(v\cdot x/2\cdot D)\cdot$$
$$\cdot K_0(v/2\cdot D\cdot\sqrt{x^2+y^2})$$

where: K_0 - Mc Donald function of order 0.
- the solution of equation (1) and voluminal efficiency (3) is, [16], :

$$(22)\qquad T(x,y,z) = T_0 + \frac{P\cdot A}{4\cdot\pi\cdot K\cdot L}\cdot \exp(v\cdot x/2\cdot D)\cdot [\frac{\exp(-v/2\cdot D\cdot R_1)}{R_1} +$$
$$+\frac{\exp(-v/2\cdot D\cdot R_2)}{R_2} + \sum_{n=0}^{\infty}\sum_{i=3}^{6}\frac{\exp(-v/2\cdot D\cdot R_i)}{R_i}].$$

Solutions (18)-(22) are the basic solutions with regard to point sources. For the extended source it is necessary to compute the convolution of the basic solution (standarized) with a load being e.g.

$$(23)\qquad T_1(x,y,z,t) = \iiint_V q(\eta, u, \xi)\,.T(x-\eta, y-u, z-\zeta, t)du\cdot d\eta\cdot d\xi$$

where: V - volume inside the layer swept by the Gaussian beam , T(x,y,z,t) - one of the solutions (18)-(22), η, u, ξ xconstants of the integration.
After transformations :

$$T_1(x,y,z,t) = \frac{L}{2\cdot N\cdot M}\cdot \sum_{m=0}^{M} w(\zeta)\cdot \sum_{k=-N}^{N}\int_{-y_{km}}^{y_{km}} q_{km}(x_{km},u,\zeta_m)\cdot$$
$$\cdot T(x-x_{km}, y-u, z-\zeta_m, t)du$$

(24) $$x_{km}^2 + y_{km}^2 = w^2(\zeta_m), \zeta_m = m \cdot L / M,$$ m,k - summing indexes.

3.2 *Stationary problem.* In case of the stationary heat conduction problem: we have from (24) for homogeneous beam distribution

(25) $$T_1(x,y) = \frac{PA}{\pi r_0^{\,2} LK} \frac{1}{2N} \sum_{i=-N}^{N} \exp[v(x-x_i)/2D] \cdot \cdot \int_{-y_i}^{y_i} K_0(v/2D\sqrt{(x-x_i)^2 + (y-u)^2})du$$

(25) $$y_i = \sqrt{r_0^2 - x_i^2},$$

and for 2D Gauss distribution [16]:

$$T_1(x,y) = \frac{2 \cdot P \cdot A}{\pi \cdot w_0^2 \cdot L \cdot K} \frac{1}{2N} \sum_{i=-N}^{N} \exp(v(x-x_i)/2D) \int_{-y_i}^{y_i} \exp[-2(u^2 + x_i^2)/w_0^2]$$

(26) $$\cdot K_0(v/2D\sqrt{(x-x_k)^2 + (y-u)^2})du,$$

and for 3D - Gauss distribution,one can obtain :

$$T_1(x,y,z) = \frac{L}{NM} \sum_{m=0}^{M} w(\zeta_m) \sum_{k=-N}^{N} \int_{-y_{km}}^{y_{km}} \frac{PA}{\pi w^2(\zeta_m)KL} \cdot$$

$$\cdot \exp\{-\frac{2}{w^2(\zeta_m)}[x_{km}^2 + u^2 + (\zeta_m - z_0)^2]\}$$

$$\cdot \exp[v \cdot (x - x_{km})/2D] \cdot \{\sum_{i=1}^{2} \frac{\exp\{-v \cdot \sqrt{(z_i - \zeta_m)^2 + (x - x_{km})^2 + (y-u)^2}/2D}{[(z_i - \zeta_m)^2 + (x - x_{km})^2 + (y-u)^2]^{1/2}}$$

(27) $$+ \sum_{n=0}^{\infty} \sum_{i=3}^{6} \frac{\exp\{-v \cdot \sqrt{[z_i|_{z=z-\zeta_m}]^2 + (x - x_{km})^2 + (y-u)^2}/2D}{\{[z_i|_{z=z-\zeta_m}]^2 + (x - x_{km})^2 + (y-u)^2\}^{1/2}}\}du.$$

In practice not the temperature distribution but the melting isoterms are important: $T(x,y,L)=T_m$ because the cutting width is defined as the double value of y coordinate of the melting isoterme in the point (x,y), where it reaches its own maximal value. For each model description there is very important the model critical velocity ,that is, the velocity for which the cutting width is equal to the laser beam width $2r_0$ or $2w_0$.

Basing on the analysis of the melting isoterms and the model critical velocity, numerical calculations have been realized for the models described

by Eqs (21), (22), (25), (26) and (27) when the main parameters of the laser cutting were changing: P, v, L and *w*.

4. Numerical results. Figures 10 and 11 shows the melting isoterms for two values of the laser beam power 700 and 900 W, two different values of the sheet velocity: 12 and 23.3 mm/s, and the sheet thickness equal to 2.5 mm. It is seen that for both these models: uniform beam and 2D Gauss distribution, doubling the sheet velocity causes the twofold decrease of the cut width. The increase of the laser beam power causes the increase of the cut width .

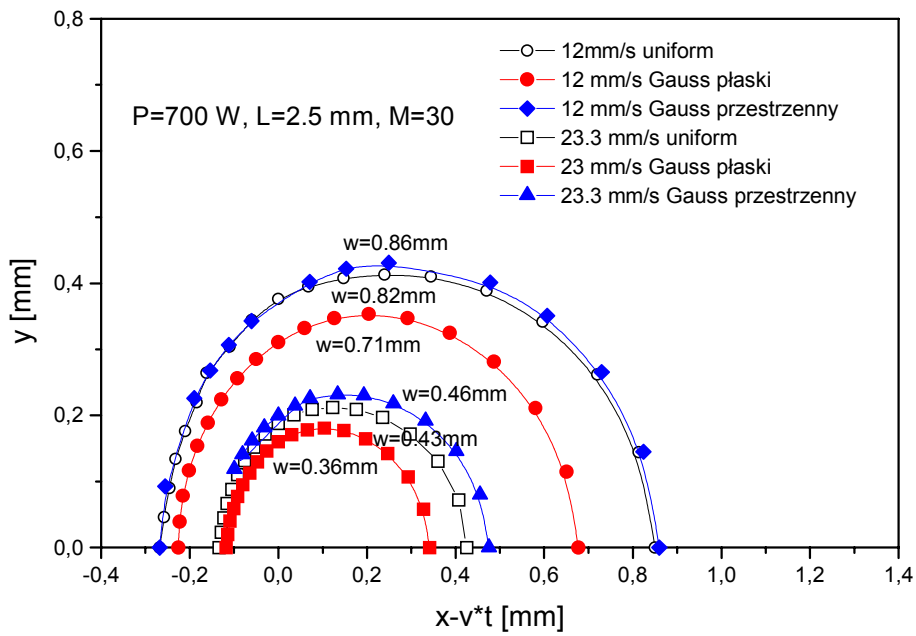

Fig.10. Melting isoterms for P = 700 W, L=2.5mm, v=12 and 23.3 mm/s and two different models: with uniform beam and 2D Gaussian distribution

Figures 12-15 show how the sheet velocity, the beam power and the sheet thickness influence the laser cutting width. In Fig.12 it is easy seen that dependences of the cutting width on the cutting velocity are hyperbolic type regardless of the model taken to account.

In Fig.13 it is seen the linear dependence of the cut width on the P/L parameter [11]. Figure 14 shows dependence of the cut width on the cutted material thickness and the cutting velocity for a uniform beam model. In Fig.15 there have been compared the numerical results with the experimental ones for the laser power 700 W. With the following measurement errors: stability of output power -4%, accuracy of power measurement up to 800W - 20W, 800-1600W - 40W, velocity measurements -6%, positioning accuracy, of x and y axes -0.25mm, z axis -0.15mm, a more accurate numerical analysis has shown that accuracy of theoretical 3D estimate is order of 40%. To obtain the greater accuracy, it is necessary to account combustion processes (additional

heat of the melting), cooling of a sheet by a assisting gas flux etc. Moreover, our technological CO_2 laser had a multimode laser beam, increasing the experimental value of *w*.

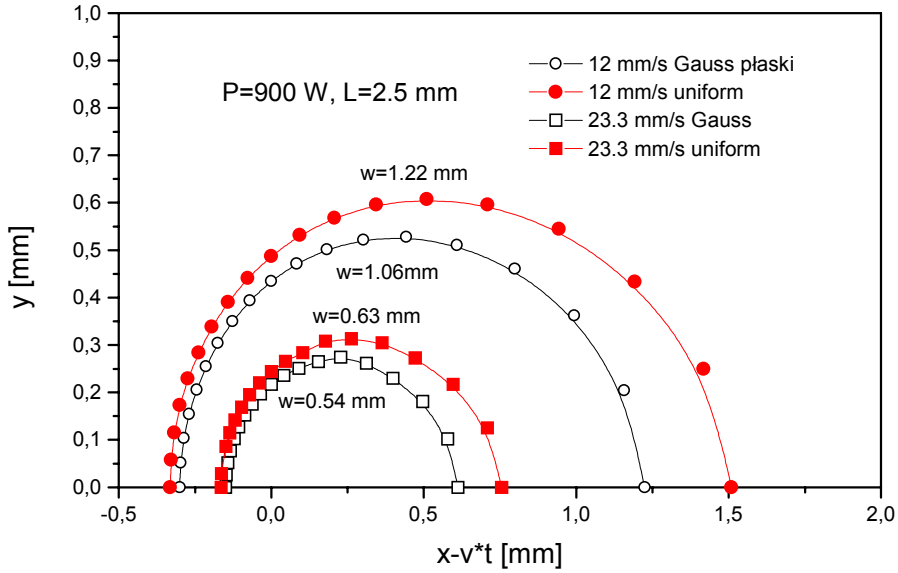

Fig.11. Melting isoterms for P=900 W and the same parameters as in Fig.10

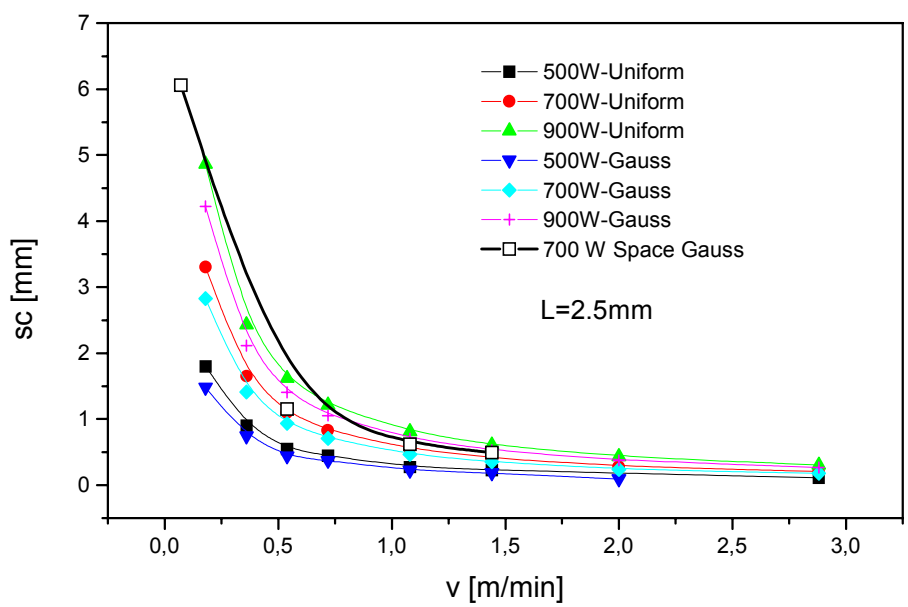

Fig.12. Change of the cutting width with the cutting velocity for P=500 , 700 and 900 W, L=2.5mm and two models: with uniform beam and 2D-Gaussian

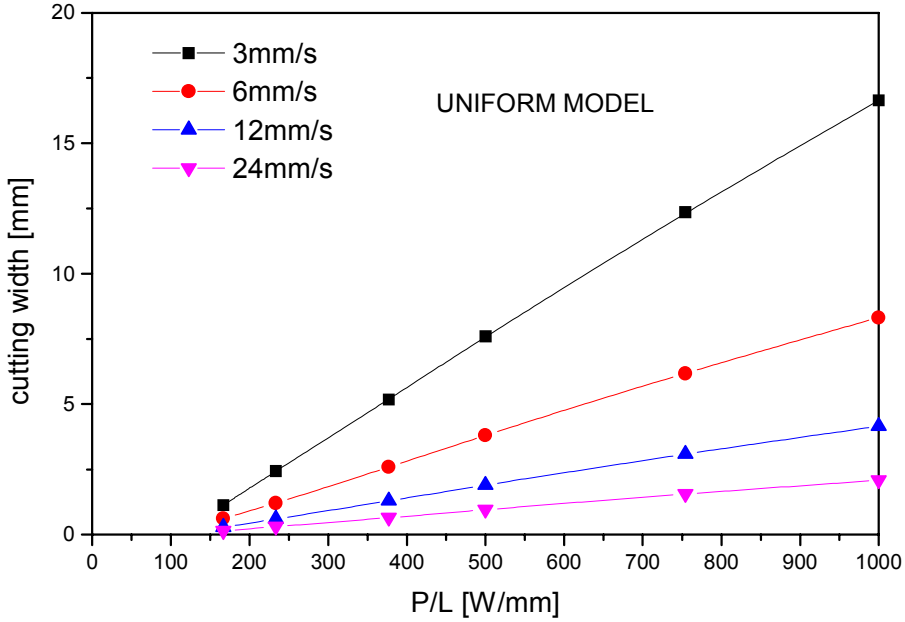

Fig.13. Change of the cutting width with the P/L parameter for different values of cutting velocities and for a uniform beam model

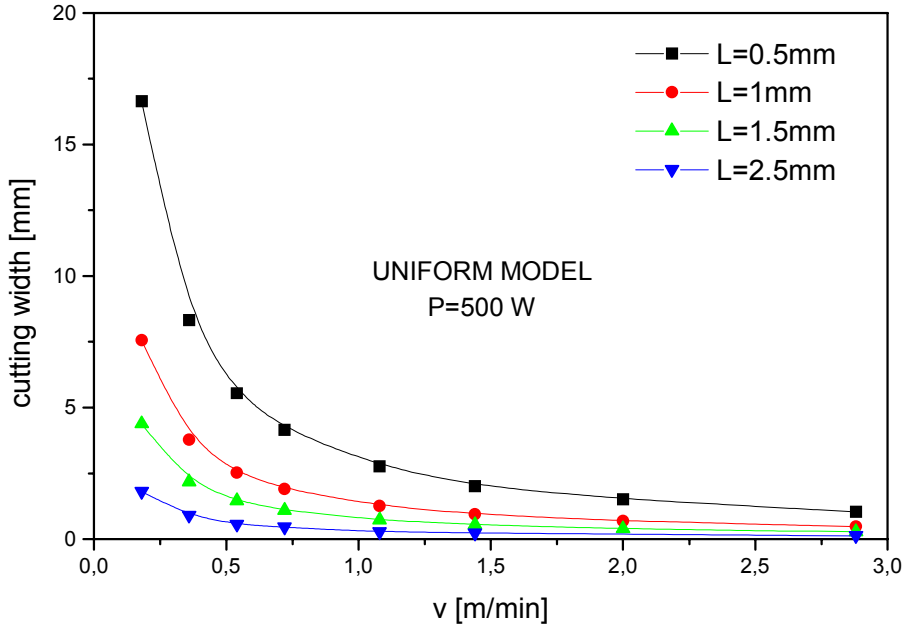

Fig.14. Change of the cutting width with a cutting velocity for different values of sheet thickness and for a uniform beam model

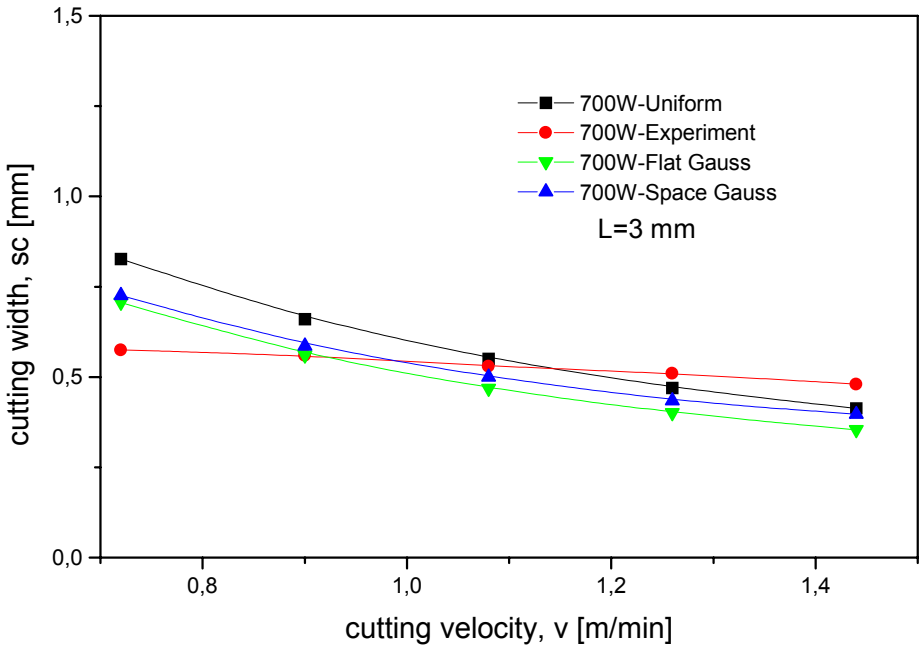

Fig.15. Comparison of the cutting width versus a cutting velocity for two models : with uniform beam and 2D- Gaussian with the experimental results [1]

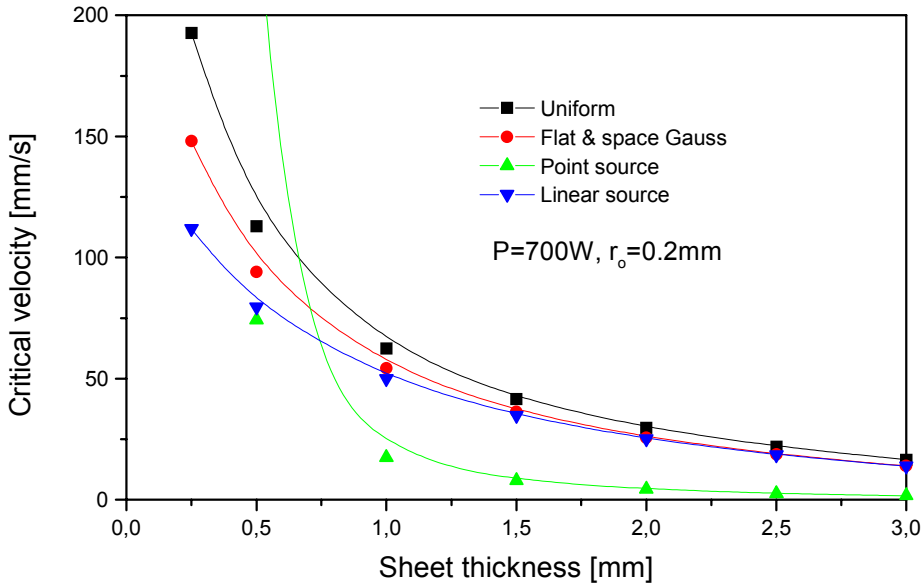

Fig.16. The critical model velocity versus the sheet thickness for P=700W and all the investigated models

Figures 16 and 17 shows the dependence of the model critical velocity on the sheet thickness and laser power respectively. As it is seen from Fig.17, results of 3D Gauss distribution model are in correspondence with the 2D

Fig.17. The critical model velocity versus the laser beam power for L=3mm and all the investigated models

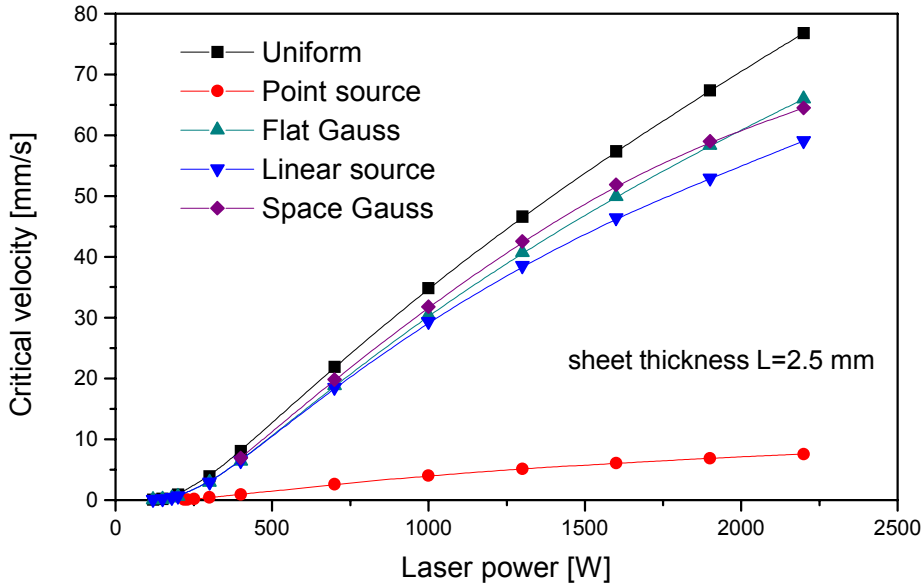

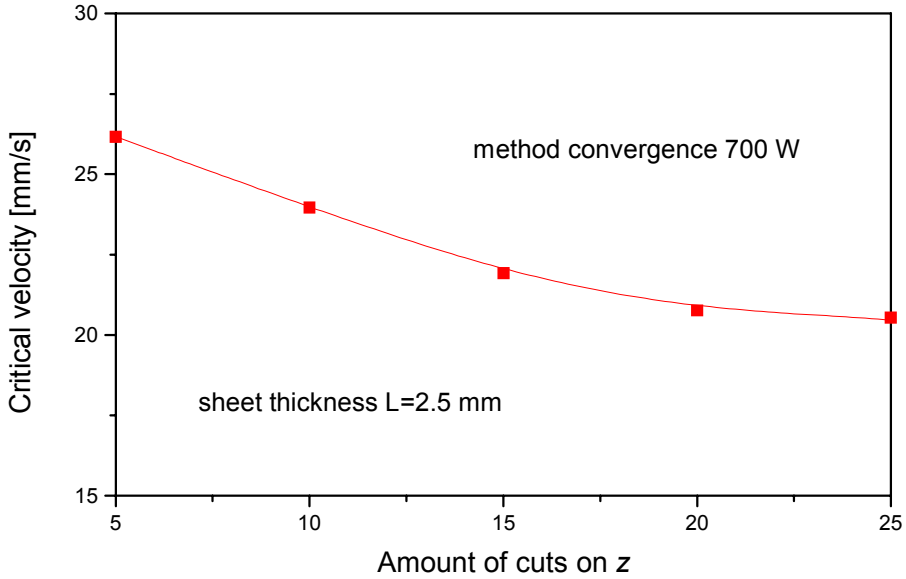

Fig.18. The critical model velocity versus the parameter M

Gauss distribution model for small values of L (=5). For L=10mm, these results correspond to these of the point source model.

In Fig.18 there are seen the changes of the critical velocity v versus the value of M according to Eq. (27). The approximation of M summing over z

axis was such that it was realized that from M=25 the parameter v was constant.

5. Conclusions. There was obtained accuracy about 40% of the theoretical results comparing to the experimental ones for a 3D Gauss distribution model. For example for the sheet of 2.5mm thickness, the experimental value of the cutting width is: experiment: 0.4<sc<0.6 mm, while the theoretical one 0.3<sc<0.5 for P=700W.

MILITARY UNIVERSITY OF TECHNOLOGY, KALISKIEGO 2, PL-00-490 WARSZAWA (WOJSKOWA AKADEMIA TECHNICZNA)

R E F E R E N C E S

[1] E. Beyer, O. Morten, K. Behler, J.M. Weick, Schneiden mit Laserstrahlung, Laser und Optoelektronik, 3 (1985) 282 - 290

[2] W. Przetakiewicz, S. Kaczmarek, A. Pawlata, J. Rafa, Analysis of the cutting effects of low carbon steels by means of technological laser, [In Polish] , Inż. Mater., 1 (1993) 19-22.

[3] A. Goldsmith, T. Waterman, H. J. Hirschorn, Handbook of thermophysical properties of solid materials, Vol.1-2, Pergamon Press, London 1961

[4] F. Richter, Die wichtigstenphysikalischen Eingenschaften von 52 Eisenwerkstoffen, Verlag Stahleisen M.B.H., Dusseldorf 1973

[5] A. Sala, Radiant properties of materials: tables of radiant values for black body and real materials, Elsevier Amsterdam 1986 and also PWN.

[6] K. Oczoœ, Lost laser treatment, [in Polish], Mech., 5 (1989), 191-196.

[7] J. Straus, Application of industrial laser CO_2, [in Polish], Przegl.Mech., 22 (1988) 5-11.

[8] W. Przetakiewicz, A. Pawlata, S.M. Kaczmarek, Cutting of Al-alloys by means of CO_2 laser- (in press).

[9] H. S. Carslow, J. C. Jaeger, Conduction of Heat Solids, Clarendon Press, Oxford 1956

[10] K. A. Bounting, G. Cornfield, Toward a general theory of cutting: A relationship between the incident power density and the cut speed, J. Heat Transfer, 2, (1975)

[11] J. N. Gonsalves, W. W. Duley, Cutting thin metal sheets with the CO_2 laser, J. Appl. Phys., 43, (1972)

[12] W. W. Duley, Laser processing and analysis of materials, Plenum Press, New York and London 1983.

[13] R. Józwicki, Lasers optics [in Polish], Wydawn. Nauk.-Tech.,Warszawa 1981

[14] S. Kaczmarek, J. Rafa, W. Przetakiewicz, A.Pawlata, “Theoretical description of cutting of steel plates by means of a coninuous wave laser CO_2", Proc. SPIE, 2202, 1994, 292 - 297

[15] L. Cagniard, Reflection and refraction of progressive seismic waves, Mc Graw-Hill Book Co., London 1962.

[16] S. Kaczmarek, J. Rafa, W. Przetakiewicz, A. Pawlata, "Theoretical models of the laser cutting of steel sheets by means of CO_2 continuous wave laser", [in Polish], Biul.Mil. Acad. Technol., 5 (1993) 29-42

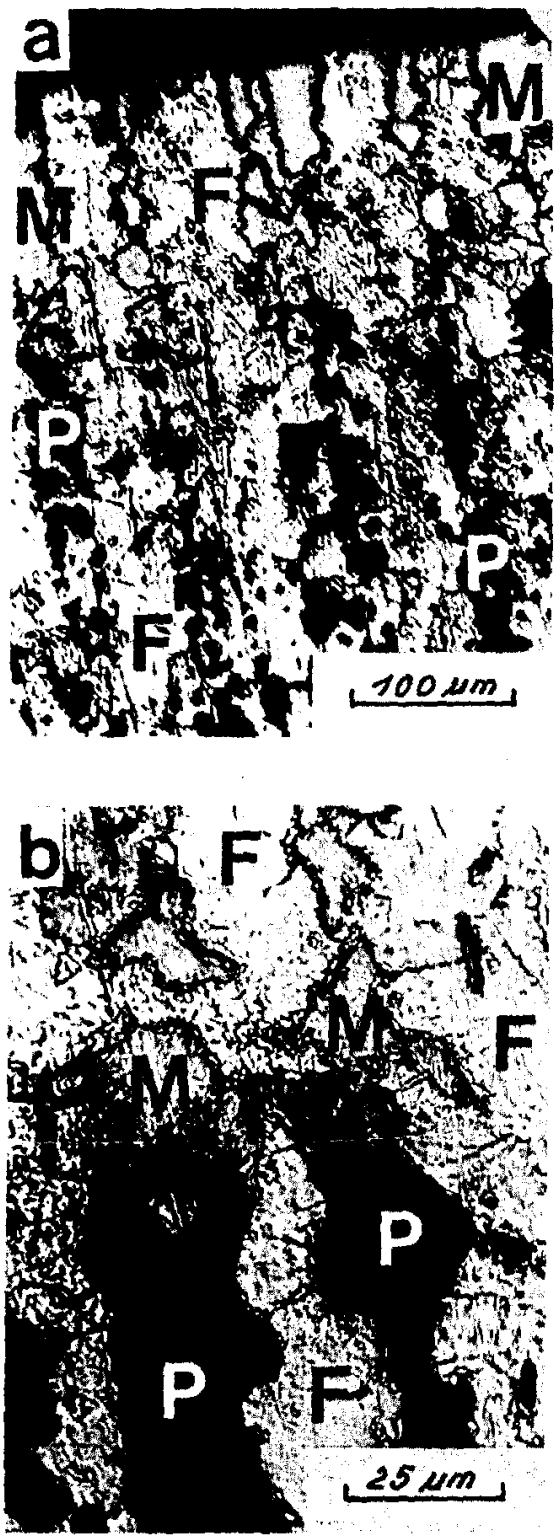

Fig. 4. Microstructure changes inside the HAZ for St3SCuX
M — martensite, *P* — pearlite, *F* — ferrite

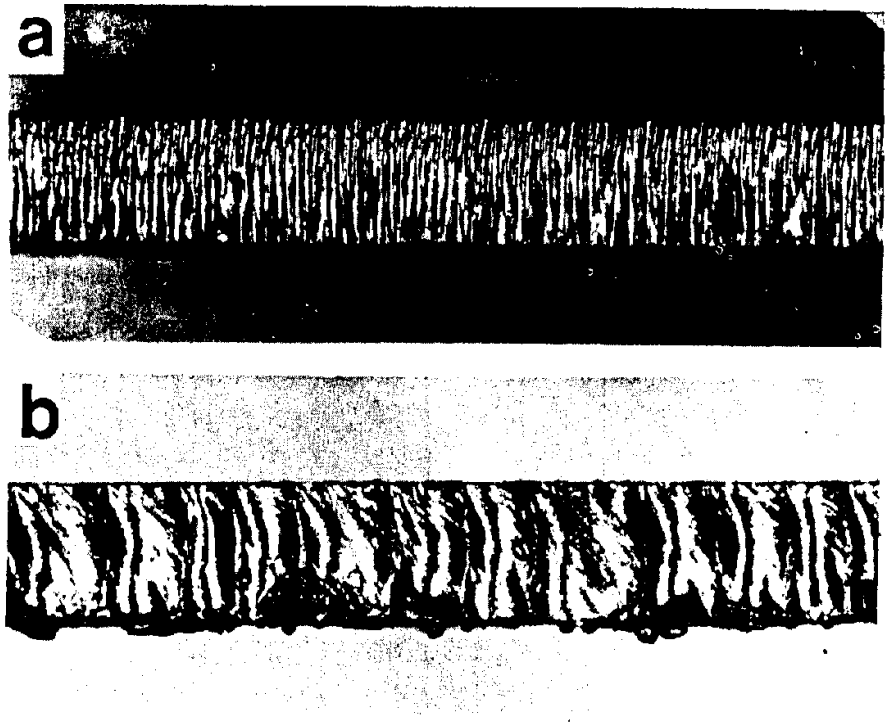

Fig. 5. Various quality of the cutting surface for St3SCuX
for beam focus positions: a — $z_0 = -0.2$ mm, b — $z_0 = +2.8$ mm

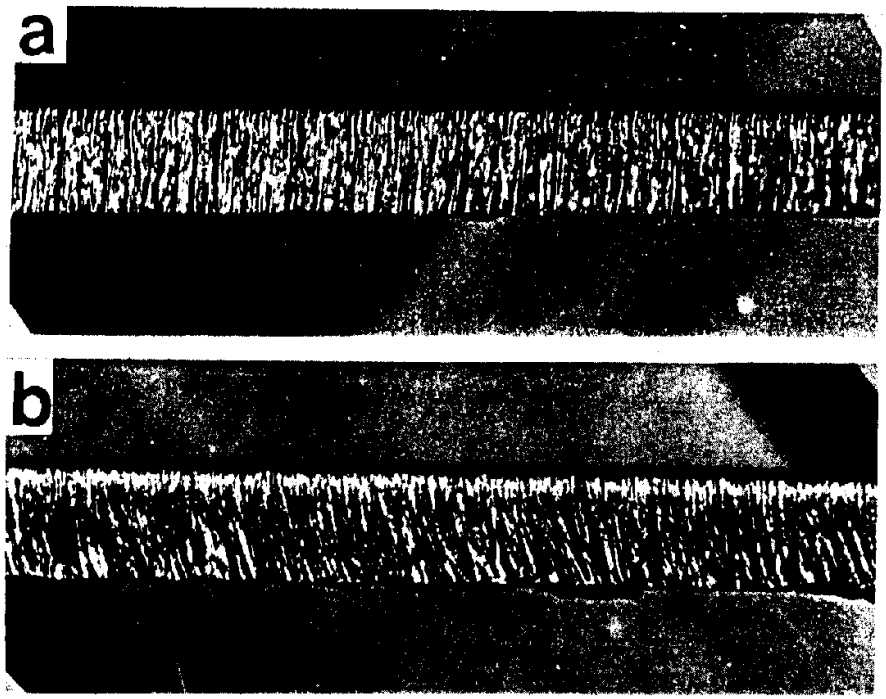

Fig. 6. Various quality of the cutting surface for MSt1:
a — $v = 1400$ mm/min, b — $v = 2000$ mm/min
$P = 700$W, $z_0 = 0.2$ mm

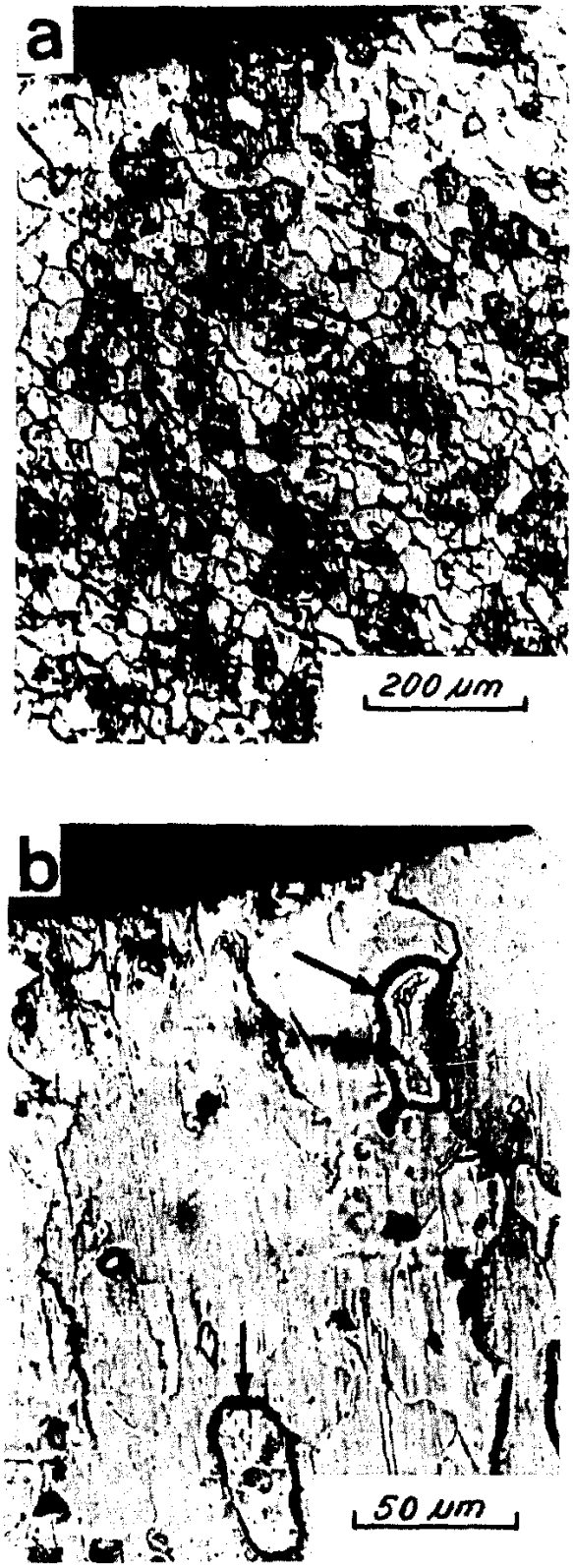

Fig. 9. Changes of the microstructure inside the HAZ for MSt1 steel
P = 900W, v = 100 mm/min, z_0 = −0.2 mm